

A Superconducting Millimetre Switch with Multiple Nano-Bridges

Boon-Kok Tan, Ghassan Yassin, Leonid Kuzmin, Ernst Otto, Hocine Merabet, and Chris North

Abstract—In this paper, we describe the design of a planar superconducting on/off switch comprising a high normal resistance nano-bridge deposited across a slotline transmission line. We present preliminary experimental results measured at 220 GHz range, and we discuss in detail the various parameters that affect the performance of the planar on/off switch, including the optimum thickness required for the nano-bridge to achieve high dynamic range and low transmission loss. The analysis is done by combining the accurate superconducting surface impedance description with rigorous electromagnetic simulations, and comparing the simulated results with the measured performance of a previously fabricated on/off switch fed by a back-to-back unilateral finline taper. Finally, we propose an improved method to further increase the dynamic range of the switch, by introducing a multi-bridge design to tune out the residual inductance of the nano-bridges.

Index Terms—Superconducting integrated circuits, system-on-a-chip, submillimeter wave devices, superconducting switches, phase modulation.

I. INTRODUCTION

AN important component for constructing an ultra-sensitive polarimeter is the fast modulating of the input signal's polarisation state. It shifts the signal frequency away from the $1/f$ noise, and separates the polarised signals from the unpolarised foreground. More importantly, it allows the measurement of both Q and U Stoke's parameters without moving the polarimeter components [1]. Several technologies has been considered for modulating the polarization signal from the sky in various astronomical instruments, including rotating quasioptical or waveguide half-wave plates and Faraday rotators [2]. However, these techniques involve the employment of moving parts, or require varying magnetic fields.

A planar phase shift circuit that can translate the rapid on/off switching mechanism into phase modulation is potentially a much more efficient and elegant solution. A planar design allows the switch to be easily integrated into the detector circuit and eventually the realisation of a fully planar receiver. Figure 1 shows how a planar phase shift circuit can be incorporated into a pseudo-correlator system to measure the polar-

B-K. Tan and G. Yassin are with the Department of Physics (Astrophysics), University of Oxford, Denys Wilkinson Building, Keble Road, OX1 3RH, Oxford, UK. E-mail: tanbk@astro.ox.ac.uk

B-K. Tan is also with the Institute for Research and Innovation, Wawasan Open University, 54 Jalan Sultan Ahmad Shah, 10050 Penang, Malaysia.

L. Kuzmin and E. Otto are with the Department of Microtechnology and Nanoscience, Chalmers University of Technology, S-41296 Gothenburg, Sweden.

H. Merabet is with the Mathematics, Statistics and Physics, Qatar University, P.O. Box 2713 Doha, Qatar.

C. North is now with the Cardiff School of Physics and Astronomy, Cardiff University, Queen's Buildings, The Parade, Cardiff CF24 3AA.

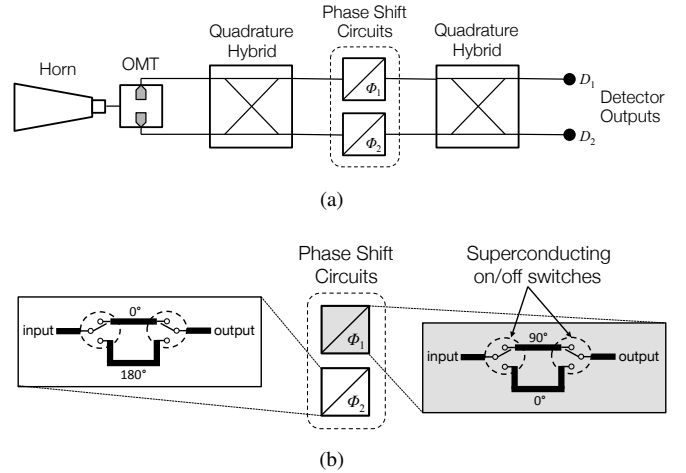


Fig. 1. (a) Schematic of a pseudo-correlator using phase shift circuits. The incoming radiation is split into two linear polarizations by the OMT, which are then combined using a quadrature hybrid to produce two circular polarizations. A phase shift circuit is used to produce a phase difference of $\Delta\phi = |\phi_1 - \phi_2|$ between the circular polarised signals, before they are recombined by another quadrature hybrid to produce two orthogonal linear polarizations. (b) Schematic drawing showing how a phase shift circuit can be constructed using two delay lines. Two on/off switches alternating in sync are utilised to select which delay line the RF signal will pass through.

ization of the sky signal. The incoming signal is split into two linear polarisations by the orthogonal mode transducer (OMT) and converted into circular polarisations via the quadrature hybrid. The two polarised signals are phase modulated with respect to each other using the phase shift circuits, before they are recombined through another quadrature hybrid to produce two orthogonal linear polarisations, and fed to the detectors D_1 and D_2 . If the input RF signal is described by the Stoke's parameters I , Q , and U , it can be shown that the outputs of the two detectors D_1 and D_2 are [3]:

$$D_1 = I - Q \cos \Delta\phi - U \sin \Delta\phi, \quad \text{and} \quad (1a)$$

$$D_2 = I + Q \cos \Delta\phi + U \sin \Delta\phi. \quad (1b)$$

When the first phase shift circuit is set to modulate between $\phi_1 = 90^\circ$ and 0° , and the second phase shift circuit modulating between $\phi_2 = 0^\circ$ and 180° , the synchronous modulation produces a phase difference of $\Delta\phi = |\phi_1 - \phi_2| = 90^\circ$ during the first half of the duty cycle and $\Delta\phi = |\phi_1 - \phi_2| = 180^\circ$ during the second half. Therefore, by taking the difference of the detector outputs $D_1 - D_2$, the linear polarisation parameters Q and U can be determine simultaneously for a single sky pixel.

Figure 1 (b) shows a conceptual sketch of a phase shift

circuit where two delay lines of different lengths are used to bridge the input and the output line. To select the desired phase delay, two on/off switches that alternate in sync between the two delay lines is required. The on/off switch can be realised by depositing a narrow strip of high residual resistance ratio (RRR) superconductor, such as Niobium Nitride (NbN) or Niobium Titanium Nitride (NbTiN), across a slotline. By changing the impedance of this nano-bridge from superconducting to normal state (and vice versa), the RF signal can be directed to either branches of the phase shift circuit. In each case, the RF signal sees two substantially different complex impedance states, hence switched from one delay line branch to another. The detail design of a planar superconducting on/off switch operating at millimetre wavelengths can be found in [4], [5] and [6]. In this paper, we focus on discussing the preliminary experimental results and the various parameters that affect the performance of the switch, including the optimum thickness required for the nano-bridge to achieve high dynamic range and low transmission loss. All the analysis presented below is done by combining the accurate superconducting surface impedance description with High Frequency Structure Simulator (HFSS).

II. PRELIMINARY EXPERIMENTAL RESULTS

Our superconducting on/off switch comprises a 22 nm thick and $0.5 \mu\text{m}$ wide NbN nano-bridge deposited across a $5 \mu\text{m}$ wide slotline, corresponding to a characteristic impedance of 69Ω . The RF signal is fed to the slotline via a unilateral finline taper, and re-radiated back to the output port via another finline, as shown in Figure 2. Both the finline taper and the nano-bridge are made out of the same superconducting

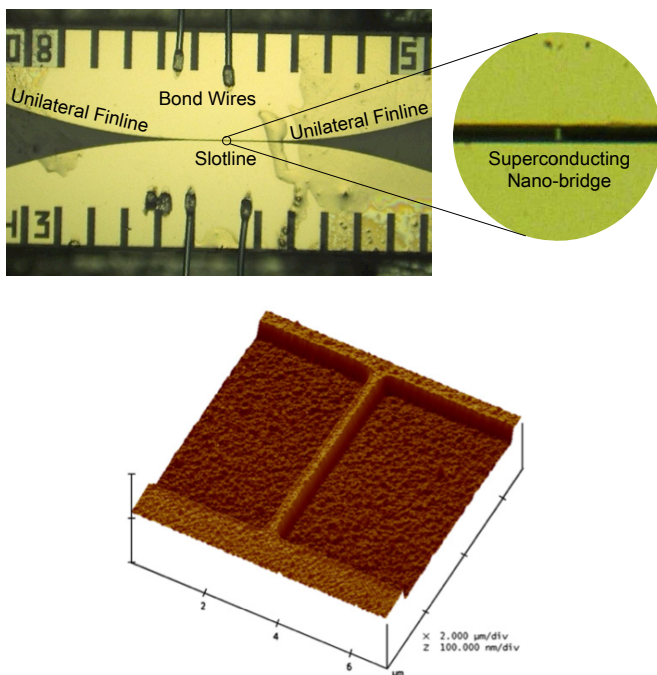


Fig. 2. A planar superconducting on/off switch comprising a superconducting nano-bridge deposited across the slotline section of a back-to-back unilateral finline taper.

material, NbN, with resistivity $\rho = 200 \mu\Omega\text{cm}$, critical current density $J_{crit} \approx 15 \text{ kA}\mu\text{m}^{-2}$, and the London penetration depth $\lambda_L = 200 \text{ nm}$. The NbN finline taper was overlaid with a thin layer of gold for bonding purposes and the whole structure is supported by a $200 \mu\text{m}$ quartz substrate. The reader is referred to [5] for the detailed description of the fabrication process.

The finline chip is positioned at the E-plane of a rectangular waveguide, and a superconductor-insulator-superconductor (SIS) device designed to operate at the frequency range of 180–260 GHz is placed after the finline chip to read the transmitted RF power. Both the finline and the SIS detector chips are housed within a split aluminium block, along the waveguide connected to a millimetre horn to couple the local oscillator (LO) signal to the finline chip, as shown in Figure 3. The nano-bridge is modulated between the superconducting (on) and the normal (off) states by applying a bias current along the nano-bridge, causing it to become normal when the bias current exceeds the critical current value. By measuring the tunnelling current across the SIS device, we can therefore obtain the response of the nano-bridge (as a switch) to the LO signal. Figure 4 shows a typical DC IV curve measured from the SIS devices, with and without the illumination of the LO signal at 207 GHz. The difference between the pumping level when the nano-bridge is biased above and below the critical current is clearly seen in the inset of Figure 4. This demonstrates that the nano-bridge is in fact acting as a switch, attenuating the LO signal coupled to the SIS detector, when the nano-bridge is in the superconducting state.

In order to reduce the $1/f$ noise, we modulated the LO signal entering the millimetre horn using a chopper wheel, and employed a lock-in amplifier to measure the output from the SIS detector. Figure 5 shows the lock-in timestream data of the SIS device output and the demodulated switching signal, at 234 GHz and 247 GHz. The nano-bridge is switched at 8.137 Hz, and the LO signal was chopped at 120 Hz. As can be seen, the response of the SIS devices is clearly corresponding to the switching of the nano-bridge. Interestingly though, the switching behaviour changes over the range of frequencies, as shown in Figure 6 (a). At some frequencies, the switching is inverted. Contrary to expectation, the power transmitted to the SIS device is lower when the nano-bridge is at normal state compared to the superconducting state i.e., $\Delta_T = S_{12,on}/S_{12,off} > 0 \text{ dB}$. An example of this is shown in Figure 5 (b) where a clear inversion effect is observed at 247 GHz. Simulation done using HFSS¹ shows the exact same effect, although in this case, the inversion occurs around 230 GHz instead of 247 GHz. Moreover, the HFSS simulation predicts a dynamic range Δ_T of around $\pm 0.5 \text{ dB}$, which is very close to the measured dynamic range of the fabricated nano-bridge device.

It is obvious from Figure 6 (a) that the main reason the tested design has a low dynamic range is because when the nano-bridge is superconducting, it does not reject the LO signal efficiently. When the switch is off (normal state), it transmits approximately -0.5 dB of power through as ex-

¹The nano-bridge is represented as a lumped element with surface impedance of both normal and superconducting states calculated using Equation 2.

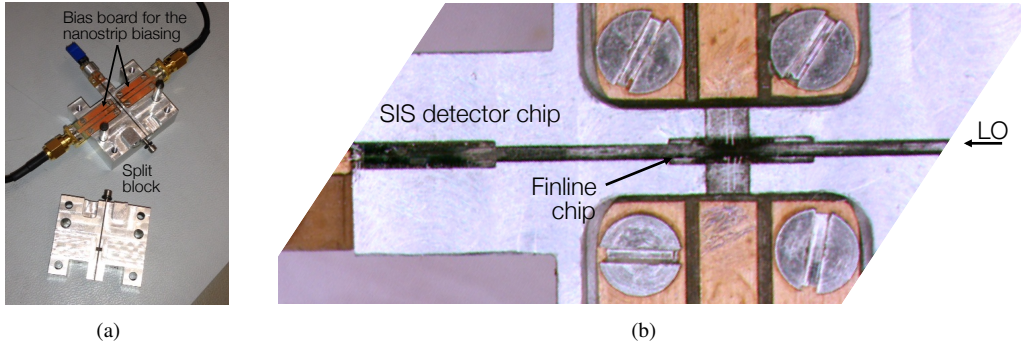


Fig. 3. (a) A split aluminium block housing both the finline and the SIS detector chips. (b) Both the SIS detector chip and the finline chip are suspended across the E-plane of a rectangular waveguide via the deep grooves in the waveguide wall. Two coplanar waveguide transmission lines are used to supply the bias current to switch the nano-bridge from superconducting to normal state. The LO signal from the left is coupled to the slotline section with the nano-bridge, and re-radiated towards the SIS detector chip via a back-to-back finline taper.

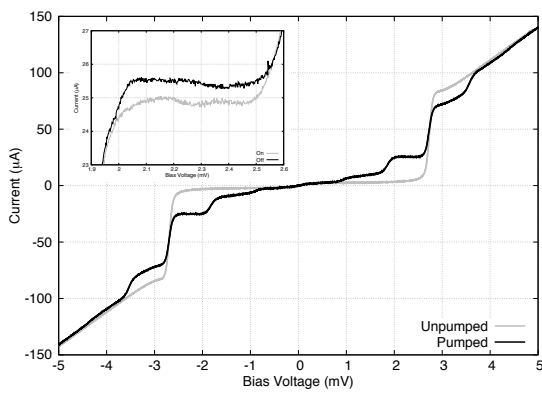


Fig. 4. An example of the DC pumped and unpumped I-V curves of the SIS device. The inset shows the changes in the tunnelling current across the first photon step, when the nano-bridge is being switched from normal to superconducting state, therefore attenuating the LO power coupled to the tunnel junction.

pected, where a negligible part of the LO power was rejected due to the finite impedance of the nano-bridge. Therefore, the main issue here is why the superconducting nano-bridge presents a relatively large impedance value that does not short the transmission line. Furthermore, at certain frequencies, the impedance presented by the nano-bridge must be higher at the superconducting state, compared to the normal state, causing the inversion effect.

The impedance of a superconducting strip is determined by the resistive part of its surface impedance R_{surf} ; the geometric inductance L_{geo} , and the kinetic inductance L_{kin} . The later inductance has a significant value only in the superconducting state, whereas $R_{surf} = R_N$, its thin film normal resistance in the normal state, and $R_{surf} \approx 0$ in the superconducting state. The value of these parameters are given by [3]:

$$R_N = \rho l / wt, \quad (2a)$$

$$L_{geo} = 0.2l \left[\frac{1}{2} + \ln \left(\frac{2l}{w+t} \right) + 0.11 \left(\frac{w+t}{l} \right) \right] \mu\text{H}, \quad (2b)$$

$$L_{kin} = \mu_0 \frac{l\lambda_L}{w} \coth \frac{t}{\lambda_L}, \quad (2c)$$

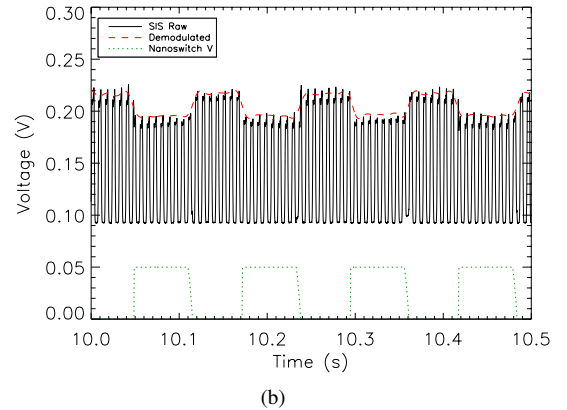
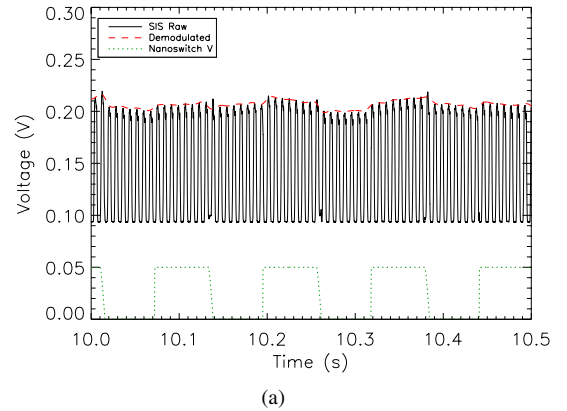
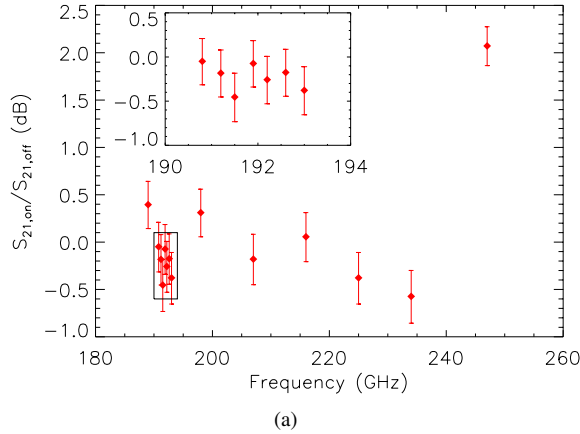


Fig. 5. Zoom in timestreams of a nano-bridge device with illumination from the LO at two frequencies: 234 GHz (top) and 247 GHz (bottom). The SIS tunnelling current is plotted as black, solid line, while the demodulated switching signal is plotted as red, dashed line. The voltage across the nano-switch is the green line at the bottom. The switching is in opposite senses at these two LO frequencies, being inverted at 247 GHz.

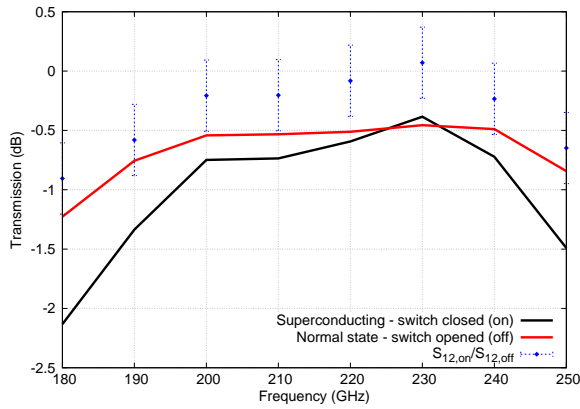
where ρ is the resistivity of the superconductor, λ_L is the London penetration depth, and w , l and t is the width, length and thickness of the superconducting strip respectively. For an RF/LO signal at an angular frequency of $\omega = 2\pi f$, the two impedance states are thus given by [3]:

$$Z_{strip,on} = i\omega(L_{kin} + L_{geo}) \quad (3a)$$

$$Z_{strip,off} = R_N + i\omega L_{geo}. \quad (3b)$$



(a)



(b)

Fig. 6. (a) The power transmission ratio of the nano-bridge device between the two states across the operating frequency range. The inset is a zoom of the ratio at a narrow frequency range. (b) HFSS simulated response of the same nano-bridge device, showing similar dynamic range and switching behaviour as the measured results. The inversion in response is observed at 230 GHz, instead of the measured 247 GHz.

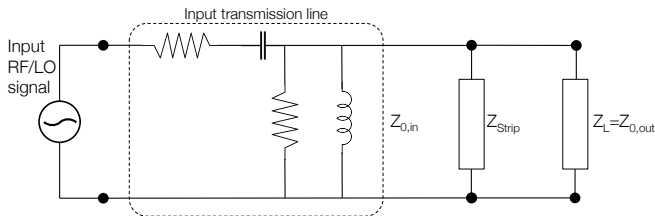


Fig. 7. Circuit diagram representing the input and output transmission line, connected with a nano-bridge across the slotline, represented by Z_{strip} .

For an ideal switch: in the superconducting ('switch-on' or closed) state, the nano-bridge has an impedance of $Z_{strip,on} \ll Z_0$, the characteristic impedance of the slotline as shown in Figure 7. In this state, the load acts as a short, and any waves propagating along the transmission line are reflected, therefore no power is transmitted to the output line. In the normal ('switch-off' or opened) state, the surface impedance is much higher ($\approx R_N$) and the nano-bridge has an impedance of $Z_{strip,off} \gg Z_0$. This act as an open in the circuit term, and the RF/LO signal will pass through the transmission line with minimum loss.

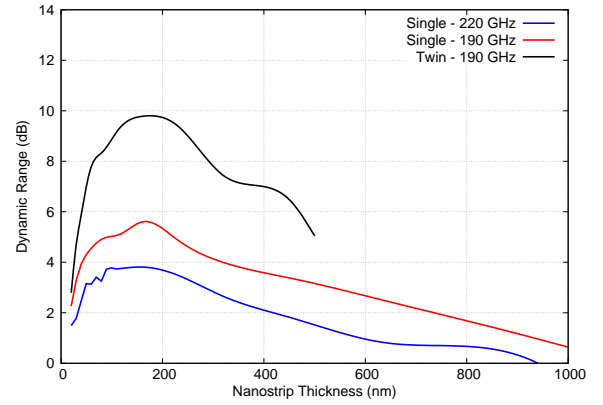


Fig. 8. The effects of the nano-bridge thickness on the dynamic range of the on/off switch.

The successful operation of the nano-bridge as a superconducting on/off switch relies on the fact that $Z_{strip,on}$ is significantly smaller than $Z_{strip,off}$. From Equation 3, one can see that this relation does not always hold true. Under certain circumstances, $i\omega L_{kin}$ could be larger or approaching R_N , causing $Z_{strip,on} \geq Z_{strip,off}$, and hence the inversion effect. From Equation 2, we can see that L_{kin} is greatly dependent on the term t/λ_L due to the exponential function in the equation. Small value of t/λ_L give rise to a large value of $\coth(t/\lambda_L)$. Therefore, we believe that the main reason the current design have a small dynamic range, and sometimes incurs the inversion effect, is because the fabricated nano-bridge is too thin, compared to the London penetration depth in the NbN thin film. This effect is especially noticeable at high frequencies, as shown in Figure 6. Take for example, the nano-bridge with the dimension of $w, l, t = 0.5 \times 5 \times 0.022 \mu\text{m}$ and $\rho = 200 \mu\Omega\text{cm}$ would have a value of $R_N \approx 9 \Omega$. At 240 GHz, and assuming $\lambda_L = 200 \text{ nm}$, $\coth(t/\lambda_L) = \coth(0.11) \approx 9$. This would give a value of $i\omega L_{kin} = 34.6 \Omega$, four times higher than R_N . In fact, as shown in Figure 8, the dynamic range of the nano-bridge as an on/off switch improves significantly when the thickness of the nano-bridge approaches $\lambda_L = 200 \text{ nm}$.

III. MULTIPLE NANO-BRIDGES DESIGN

It is obvious that the next generation of the on/off switch design must employed a thicker NbN nano-bridge to reduce the surface impedance in the superconducting state. However, as shown in Figure 8, the dynamic range of a $t \rightarrow \lambda_L$ nano-bridge is still limited to around 5 dB. The dynamic range of the planar superconducting on/off switch can be improved by depositing multiple nano-bridges along the slotline. The utilisation of the multi-bridge design have a two fold effects. First, the length of the transmission line between the nano-bridges can be optimised so that the complex impedance of one nano-bridge is transformed to the complex conjugate impedance of the other nano-bridge, and therefore to tune out the residual kinetic inductance of the nano-bridges. This is largely similar to the twin-junction tuning network used for cancelling out the junction capacitance of an SIS mixer [7], [8]. As shown in Figure 8, by employing two nano-bridges

separated by $50 \mu\text{m}$ slotline, we can double the dynamic range of the switch to about 10 dB.

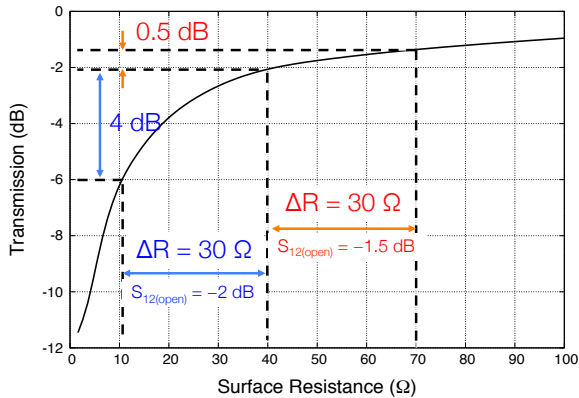


Fig. 9. The non-linear relation between the surface impedance of the nano-bridge and the power transmission. The was simulated using the HFSS model of a single $l, w, t = 5 \times 0.5 \times 0.02 \mu\text{m}$ nano-bridge as the switch.

Secondly, by using a multi-bridge scheme, the total impedance of the switch seen by the RF/LO signal at both states, $Z_{strip,on}$ and $Z_{strip,off}$, can be altered, giving a degree of freedom for selecting the optimum operating point of the switch. As shown in Figure 9, the power transmission allowed by the switch depends on the impedance of the nano-bridge/s, and the relation is non-linear. This indicates that the dynamic range of the switch relies heavily on the difference of the nano-bridges resistances between the two switching states. From the plot, it is clear that the dynamic range improves with the lower impedance values, but this also results in lower power transmission when the switch is in the normal state (‘switch-off’). For example, if the difference in impedance between the superconducting and the normal state are $\Delta R = |R_{normal} - R_{super}| = 30 \Omega$, where R_{normal} is 40Ω and R_{super} is 10Ω , the dynamic range is about 4 dB. However, in this scenario, when the switch is off, it only allows -2 dB of power transmission. In order to improve the power transmission at the switch-off state, we can operate the switch at say 70Ω , giving a transmission of approximately -1.5 dB . However, if we retain the same $\Delta R = 30 \Omega$ difference², one notice immediately that the dynamic range drops by 8-folds. Therefore, there is an unavoidable compromise between the optimum dynamic range achievable and the allowed power transmission when the switch is off.

Figure 10 shows a HFSS simulated model of two and three nano-bridges deposited to form the on/off switch. Each nano-bridge is $0.5 \mu\text{m}$ wide, $5 \mu\text{m}$ long and is formed using a 50 nm thick NbN film. The nano-bridges are separated by a $50 \mu\text{m}$ long slotline, and fed by a back-to-back unilateral finline taper as described before. Figure 10 (c) shows the HFSS predicted power transmission and dynamic range behaviour of the on/off switch with one, two and three nano-bridge/s. As can be seen, the dynamic range improves almost linearly with the number

²The reason behind this is that if R_N is increased to give a higher R_{normal} value by say making the nano-bridge longer, it will inevitably increase the value of L_{kin} as well, thus higher value of R_{super} . Therefore, ΔR always remain almost the same regardless of the switch-off impedance operating point of the switch.

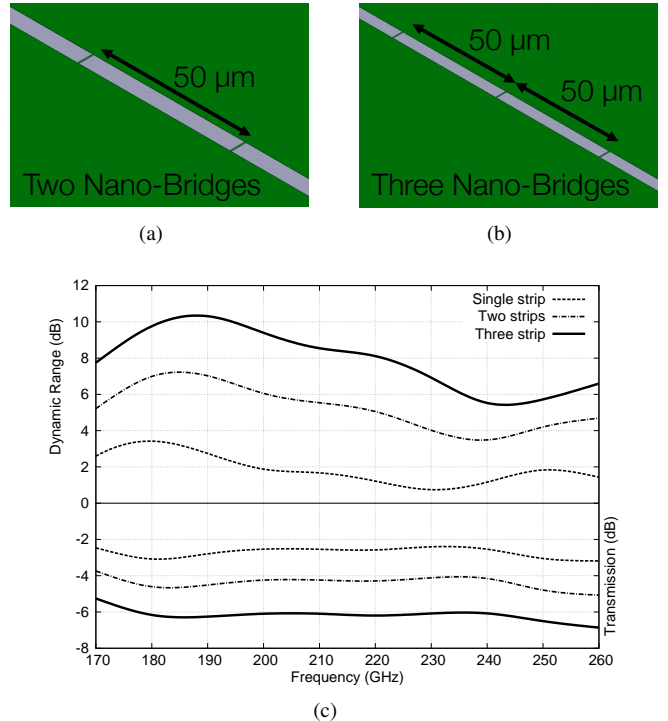


Fig. 10. (a) & (b) Examples of the multi-bridge design, where two and three nano-bridges are deposited along the transmission line, separated by a $50 \mu\text{m}$ long slotline. The nano-bridges are 0.5μ wide, $5 \mu\text{m}$ long and 50 nm thick. (c) The power transmission allowed by the multi-bridge switch during the switch-off state, and the dynamic range, of the one-, two- and three-bridges design.

of nano-bridges, but at the same times, the transmission in the off-state drops almost proportionally as well. Hence, for a specific application, the designer should carefully chosen the number of nano-bridges and the dimension of the nano-bridge, to find a balance between the dynamic range required and the transmission loss.

IV. CONCLUSION

We have presented a design of a planar superconducting on/off switch utilising a nano-bridge connecting the two electrodes of a slotline. The preliminary experimental results have been presented and discussed in detail, especially the various parameters that affect the performance of the switch. The most important result from the discussion is that the tested nano-bridge is too thin, therefore preventing the nano-bridge to present low impedance when it is biased below the critical current value. In this paper, we have also proposed a new design that can improve the dynamic range of the switch, by utilising multiple nano-bridges along the same slotline. We have shown that by carefully choosing the separation distance between the nano-bridges, we can improve the dynamic range by two fold. We are currently in the process of fabricating a new batch of superconducting on/off switch using the new multi-bridge design with a thicker NbN film, and the experimentally obtained results from testing these devices will be reported.

REFERENCES

- [1] C. North, “Observations of the cosmic microwave background polarization with *clover*,” Ph.D. dissertation, University of Oxford, Oxford, United Kingdom, 2010.
- [2] P. A. R. Ade, D. T. Chuss, S. Hanany, V. Haynes, B. G. Keating, A. Kogut, J. E. Ruhl, G. Pisano, G. Savini, and E. J. Wollack, “Polarization modulators for CMBPol,” *Journal of Physics Conference Series*, vol. 155, no. 1, p. 012006, Mar. 2009.
- [3] G. Yassin, P. Kittara, A. Jiralucksanawong, S. Wangsuya, J. Leech, and M. Jones, “A High Performance Horn for Large Format Focal Plane Arrays,” in *Proceedings of the Eighteenth International Symposium on Space Terahertz Technology*, 2007, pp. 199–+.
- [4] P. K. Grimes, G. Yassin, L. S. Kuzmin, P. D. Mauskopf, E. Otto, M. E. Jones, and C. E. North, “Investigation of planar switches for large format CMB polarization instruments,” in *Society of Photo-Optical Instrumentation Engineers (SPIE) Conference Series*, ser. Society of Photo-Optical Instrumentation Engineers (SPIE) Conference Series, vol. 6275, Jul. 2006.
- [5] G. Yassin, L. S. Kuzmin, P. K. Grimes, M. Tarasov, E. Otto, and P. D. Mauskopf, “An integrated superconducting phase switch for cosmology instruments,” *Physica C Superconductivity*, vol. 466, pp. 115–123, Nov. 2007.
- [6] L. Kuzmin, M. Tarasov, É. Otto, A. Kalabukhov, G. Yassin, P. Grimes, and P. Mauskopf, “Superconducting subterahertz fast nanoswitch,” *Soviet Journal of Experimental and Theoretical Physics Letters*, vol. 86, pp. 275–277, Oct. 2007.
- [7] V. I. Belitskii, M. A. Tarasov, S. A. Kovtoniuk, L. V. Filippenko, and O. V. Kaplunenko, “Low noise completely quasioptical SIS receiver for radioastronomy at 115 GHz,” *International Journal of Infrared and Millimeter Waves*, vol. 13, pp. 389–396, Apr. 1992.
- [8] P. Grimes, “Design and analysis of 700 GHz Finline Mixers,” Ph.D. dissertation, University of Cambridge, United Kingdom, 2006.